Collective excitations and low-temperature transport properties of bismuth

P. Chudzinski and T. Giamarchi
DPMC-MaNEP, University of Geneva, 24 Quai Ernest-Ansermet CH-1211 Geneva, Switzerland
(Received 23 March 2011; revised manuscript received 24 June 2011; published 6 September 2011)

We examine the influence of collective excitations on the transport properties (resistivity and magneto-optical conductivity) for semimetals, focusing on the case of bismuth. We show, using a random-phase approximation (RPA), that the properties of the system are drastically affected by the presence of an acoustic-plasmon mode, which is a consequence of the presence of two types of carriers (electrons and holes) in this system. We find a crossover temperature T^* separating two different regimes of transport. At high temperatures where $T > T^*$, we show that Baber scattering explains quantitatively the dc resistivity experiments, while at low temperatures where $T < T^*$, the interactions of the carriers with this collective mode lead to a T^5 behavior of the resistivity. We examine other consequences of the presence of this mode, and in particular predict a two-plasmon edge feature in the magneto-optical conductivity. We compare our results with the experimental findings on bismuth. We discuss the limitations and extensions of our results beyond the RPA, and examine the case of other semimetals such as graphite or 1T-$TiSe_2$.

DOI: 10.1103/PhysRevB.84.125105 PACS number(s): 72.10.Di, 71.45.Gm, 71.35.Lk, 78.20.Bh

I. INTRODUCTION

Bismuth is a material which plays an important role in solid-state physics. Due to an extremely small Fermi surface, this material provides the remarkable possibility to observe strong effects induced by the presence of external fields, i.e., pressure and temperature, even if these external forces are of moderate amplitude. Several important phenomena, i.e., the Shubnikov-de Haas[1] and de Haas-van Alphen[2] effects, have been observed in bismuth. In the last few years, a series of experiments has once again drawn the attention of the community to elemental bismuth and challenged our understanding of this material. High-pressure optical spectroscopy measurements indicate that the mechanism of semimetal-to-semiconductor decay is not fully understood.[3] Reflectivity measurements[4] showed large changes in the plasmon frequency and anomalous midinfrared features, indicating strong scattering of the electronic degrees of freedom by a plasmon collective mode. An extremely strong Nernst signal with unusual temperature dependence (both at low[5] and high[6,7] fields) was also reported.

These recent experiments clearly indicated that the question of transport in bismuth was still not understood. In fact, similar questions still existed for the standard resistivity as well. The majority of the resistivity experiments had been done in the late 1970s, including the works of Hartmann,[8] Kukkonen,[9] and later studies,[10] which showed that down to 4 K, the Fermi-liquid theory (with components of very different masses) works quite well. The T^2 resistivity behavior at lowest temperatures was explained within this theory.[9,11] However, the discussion was not closed because one year later more detailed, lower-temperature data by Uher[12] was published, which showed a significant deviation from expectations: the T^2 behavior changes smoothly into a T^5 behavior at the lowest temperatures. A quite complex theory involving coupling to a particular group of phonons was proposed as an explanation for this result.[13] We will briefly describe it in the beginning of Sec. III.

The purpose of this work is to reexamine the theory of transport in semimetals. We show that these anomalous transport properties have a simple explanation. They come from the fact that the coupling between electrons and holes with very different masses induces many-body corrections to the Fermi-liquid picture. In fact, the above-mentioned change in the resistivity was an overlooked example of how interactions in semimetals modify the simple Fermi-liquid picture. Although our study is mostly focused on bismuth, we also examine other materials which have recently been the subject of intensive studies, such as graphite[14,15] and 1T-$TiSe_2$.[16,17]

The structure of this paper is as follows. In Sec. II, we introduce the model of interaction between the electrons and holes. We show that at low temperatures, a collective acoustic-plasmon mode exists[18] and plays a central role in the properties of the material. The existence of acoustic plasmon was studied before in the context of semimetals,[19–21] but not including the possible consequences of its existence. We discuss also the high-temperature regime of conductivity and show that the Baber mechanism[22] is the dominant source of resistivity in this regime. We then examine, in Sec. III, the low-temperature regime for the resistivity. We develop an effective theory for this regime and derive a new $\rho(T)$ dependence, which is a direct consequence of the existence of a collective acoustic-plasmon mode. We examine the magneto-transport in Sec. IV. We show, in particular, that a double-plasma edge must exist. A discussion of the validity of the approximations used to derive the above-mentioned results is indicated in Sec. V, and conclusions are given in Sec. VI. Some technical details can be found in the appendices.

II. MECHANISM OF RESISTIVITY

A. Band structure and Hamiltonian

The peculiarity of bismuth comes from the very small characteristic energy scales of its Fermi liquid (see Fig. 1).

This stems from a slightly distorted, cubic crystal structure (the distortion angle is smaller than 3°). In the absence of distortion, bismuth would be a band insulator, but instead it is a quite rare rhombohedral space group $A7$ (without inversion

symmetry). Bismuth becomes a semimetal with very small amounts of fermions active at accessible energies.

The Hamiltonian of those carriers close to Fermi energy in bismuth reads, in general,

$$H = H_0^h + \sum_{\nu=1}^{3} H_0^{e\nu} + H_{int}^{h-h} + H_{int}^{e-e} + H_{int}^{e-h}. \quad (1)$$

In the above, h denotes a hole pocket, while there are three electron pockets denoted by $e\nu$. The first two terms are the free fermion kinetic energies. We approximate the kinetic energy of each type of carrier by a free dispersion relation,

$$\xi^{\alpha}(k) = \sum_{i=1}^{3} \frac{\hbar^2 k_i^2}{2m_i^{\alpha}} - E_F^{\alpha}, \quad (2)$$

where α denotes the species, the index i are the three principal axes of the energy ellipsoid (see Fig. 1), m_i^{α} is the mass tensor, the k are the momenta centered on the corresponding pocket, and E_F^{α} is the Fermi energy of the corresponding species. The values of the parameters are summarized in Table I. The huge mass ratio between different carriers (and along different axes)

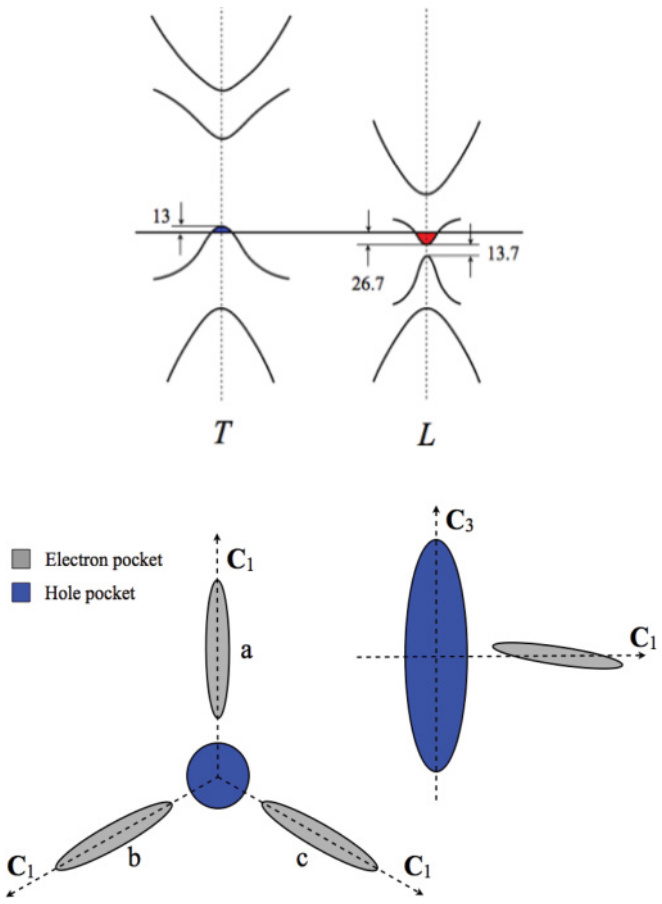

FIG. 1. (Color online) A sketch of the band structure of bismuth: three electron pockets and a central hole pocket. Top: the energy dispersion. Energies are in meV. Bottom: the four pockets. The scale is grossly exaggerated. In fact, k_F are 10^4 smaller than intrapocket distances. The electron pockets are slightly tilted out of the bisectrix-binary plane C_1-C_2 perpendicular to the trigonal axis C_3. Figure modeled after Ref. 23.

TABLE I. The band parameters of bismuth, according to Ref. 24. Masses are in units of the mass of the electron, and wave vectors are in units of reciprocal length 1.386 $\AA^{-1}$. The values are given along the principal axes of the ellipsoids, as defined in Fig. 1.

	m_1	k_{F1}	m_2	k_{F2}	m_3	k_{F3}
Holes	0.067	0.01	0.067	0.01	0.612	0.03
Electrons	0.198	0.06	0.0015	0.005	0.0021	0.005

enables us to define, in general, rapid and slow carriers, which is a notion that will be used frequently in this work. We want to emphasize that this peculiar band structure was computed quite accurately and this result was later confirmed by many experimental probes.

The latter terms in (1) are interactions whose influence is the subject of this study. We divided the interactions into three groups: hole-hole, electron-electron, and electron-hole. Each one of these terms has the form

$$H_{int}^{\alpha-\beta} = \sum_q V^{\alpha\beta}(q)\rho_{\alpha}(q)\rho_{\beta}(-q), \quad (3)$$

where α,β runs among the species. The density operators $\rho_{\alpha}(q)$ are given by

$$\rho_{\alpha}(q) = \sum_k c_{\alpha,k+q}^{\dagger} c_{\alpha,k}, \quad (4)$$

where the $c^{\dagger}$,c are the standard fermionic creation and destruction operators, and a summation overs the spin degrees of freedom is implicit. The interaction potential is the long-range Coulomb potential

$$V_{\text{Coul}}^{\alpha\beta}(q) = \frac{e_{\alpha}e_{\beta}}{\epsilon_{\infty}q^2}, \quad (5)$$

where the hole charge is the opposite of the electronic one, $e_h = -e_e$, and ϵ_{∞} is the dielectric constant due to the rest of the material. Because of the very small size of the pockets and the large distance in momentum space among them all, interactions which imply a transfer of particle from one pocket to the other must occur with a large momentum transfer. These terms are thus potentially strongly suppressed compared to the intrapocket interactions given the long-range nature of the Coulomb potential (5).

B. Screened Coulomb interaction: Acoustic plasmon

The smallness of the bismuth Fermi surface shown in Fig. 1 and incorporated in the first two terms of the Hamiltonian (1) has certain nontrivial implications for the transport properties. When $k_F^{-1} \approx 10^4$ Å, the interaction with angstrom size impurities is strongly reduced. The probability of intrapocket umklapp scattering is also very low. Since the Debye temperature for Bi is around 150 K, it implies that at $T \sim 1$ K, phonon influence will be rather weak. Moreover, thermal transport is proven experimentally to be ballistic. No evidence of any additional order parameter generating quasiparticles on which carriers could scatter has been found in the many decades of careful study of this element. Thus, in order to understand the transport properties, we can restrict ourselves to the Fermi-liquid part of the problem described by the Hamiltonian (1).

Given the above points, the main type of scattering entering resistivity should be the so-called Baber scattering,[22] coming from the presence of several types of carriers of different masses. In such a case, the conservation of momentum does not necessarily lead to the conservation of current, thus carrier collisions can produce a finite resistivity, even without umklapp processes. In contrast, with all of the above-mentioned scattering processes, Baber scattering is strongly favored by the band structure of Bi, with the ratio of electrons and holes masses being, in some directions, more than a factor of 10. The resistivity in bismuth is thus linked directly to the electron-hole interaction term in (1).

Although the bare form of such a term is given by (3), the presence of the two species of carriers leads to a strong renormalization of the bare Coulomb interaction due to dynamical screening. We thus need to examine the effects of screening on the interaction potential $V^{\alpha\beta}(q)$. Normally we have a tensor structure for the screened interaction (or alternatively the dielectric constant), but if we assume that the longitudinal and transverse modes do not mix,[25] then we can use the standard random phase approximation (RPA) for the Coulomb potential. In the presence of two types of carriers, the RPA equations are indicated in Fig. 2.

The equation of Fig. 2 can be solved by first doing the resummation on one of the species:

$$\tilde{V}^{ee}(q,\omega) = \frac{V^{ee}_{\rm Coul}(q)}{1 - V^{ee}_{\rm Coul}(q)\Pi_{hh}(q,\omega)}, \tag{6}$$

where $\Pi_{hh}(q,\omega)$ is the retarded density-density correlation function for the holes, including the interactions that are not already present in the RPA chain of bubbles of Fig. 2. The simplest and usual approximation for Π_{hh} consists of taking the free correlation $\Pi^0_{hh}(q,\omega)$. Using the Hamiltonian (1), one has

$$\Pi^0_{hh}(q,\omega) = \frac{1}{\Omega}\sum_k \frac{f(\xi(k)) - f(\xi(k+q))}{\omega + \xi(k) - \xi(k+q) + i\delta}, \tag{7}$$

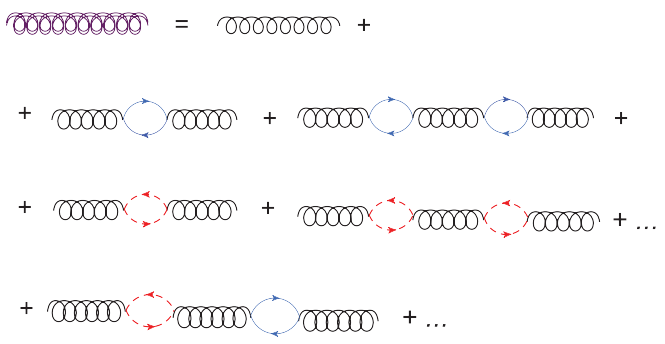

FIG. 2. (Color online) The RPA series for effective interactions for the case of a two-component system. We denote generically these components by r (rapid or fast) and s (slow). In the above diagram, the thick coil is the screened effective interaction $V_{\rm eff}(q,\omega)$, the solid blue line denotes using the standard diagrammatic convention of a fast particle, while the dotted red line is a slow particle. The black coil is the bare Coulomb potential (5).

where Ω is the volume of the system, f are the Fermi factors, and $\delta = 0^+$. Using this expression, one can get the screening of the electron-electron potential,

$$V^{ee}_{\rm eff}(q,\omega) = \frac{\tilde{V}^{ee}(q)}{1 - \tilde{V}^{ee}(q,\omega)\Pi_{ee}(q,\omega)}, \tag{8}$$

where $\Pi_{ee}(q,\omega)$ denotes the sum over the three electron pockets of the corresponding retarded density-density correlation $\Pi_{ee}(q,\omega) = \sum_{\nu=1}^{3}\Pi_{ee,\nu}(q,\omega)$. The expression (8) can be rewritten as

$$V^{ee}_{\rm eff}(q,\omega) = \frac{V^{ee}_{\rm Coul}(q)}{1 - V^{ee}_{\rm Coul}(q)[\Pi_{hh}(q,\omega) + \Pi_{ee}(q,\omega)]}, \tag{9}$$

where, in a similar way to that for the holes, one can approximate the correlation function by its free (or Fermi-liquid) value.

As can be seen from (9), a strong resonance in $V^{ee}_{\rm eff}(q,\omega)$ exists when the denominator is small, which indicates the presence of a collective mode. As usual, the dispersion relation of the mode is given by

$$1 = V^{ee}_{\rm Coul}(q){\rm Re}[\Pi_{hh}(q,\omega) + \Pi_{ee}(q,\omega)], \tag{10}$$

where Re denotes the real part. The imaginary part gives the damping of the mode. As is well known[18–20] for the case of a two-component system, Eq. (10) has two solutions. One is the standard optical plasmon, but a second one is an acoustic mode,

$$\omega_{ac} = uq = (c_{ac} - \imath\tau^{-1})q,$$

where ${\rm Re}[u] = u' = c_{ac}$ is the acoustic-plasmon velocity and ${\rm Im}[u] = u'' = -\tau^{-1}$ is the damping of the mode. For the case of isotropic Fermi surfaces with the same Fermi wave vector for the two species (neutrality condition), and one heavy m_s and light masses m_r (for slow and rapid carriers, respectively), such that $(V_{Fs}/V_{Fr})^2 \ll 1 \ll m_s/m_r$, where the V_{Fi} $(i = r,s)$ are the respective Fermi velocities k_{Fi}/m_i with $E^i_F = k^2_{Fi}/(2m_i)$ in the zeroth-order approximation (extreme mass difference), one has

$$c^0_{ac} = \sqrt{V_{Fr}V_{Fs}/3}, \tag{11}$$

and

$$(\tau^0)^{-1} = \pi V_{Fs}/12. \tag{12}$$

Physically, such an acoustic plasmon comes from the fact that for two different velocities, one of the species (the light one) will have a much larger Fermi velocity than the acoustic-plasmon mode. In that case, the corresponding $\Pi_{rr}(q,\omega)$ essentially tends to a constant $\Pi_{rr}(q \to 0,\omega = 0)$, which is the density of states at the Fermi level. This mode is fast enough to screen the Coulomb interaction. Equation (6) would just become

$$\tilde{V}^{rr}(\omega = c_{ac}q \to 0) = \frac{1}{-\Pi_{rr}(\omega = c_{ac}q \to 0)}, \tag{13}$$

transforming the original long-range interaction into a short-range one. Using the well-known result for the Lindhard function, one gets

$$-\Pi_{rr}(\omega = c_{ac}q \to 0) = \frac{m_r k_{Fr}}{\pi^2} + \imath\frac{m_r^2 c_{ac}}{2\pi}. \tag{14}$$

For the heavy mode, one is in the opposite limit, $c_{ac} \gg V_{Fs}$, for which the Lindhard function is approximately

$$-\Pi_{ss}(\omega = c_{ac}q \to 0) = \frac{m_s k_{Fs}}{\pi^2}\frac{k_{Fs}^2}{3c_{ac}^2 m_s^2}. \tag{15}$$

Substituting (13) into (8), one gets the results (11) and (12).

Such collective excitation has been already investigated in several systems,[18,19,21] but is normally very elusive. It exists usually very close to the single-particle excitation spectrum, so it can be easily Landau *overdamped*. There were proposals[26] suggesting its measurability in artificial one-dimensional (1D) systems (quantum wires), but even then its intensity was shown to be much weaker than the optical plasmon and was easily suppressed by disorder. However, we claim in the present paper that such a collective mode plays an important role in bismuth. The precise calculation of its parameters c_{ac} and τ is singularly complicated, given the complexity of the Fermi surface and the presence of the various masses. Nevertheless, we give, in Appendix A, arguments for the existence of such a mode. Mostly we will proceed along the lines that such a mode exists and explore the consequences for the various transport properties.

Note that the mode never exists as a perfectly sharp mode because of the damping (12), which always gives a finite width of the order of τ^{-1} to this acoustic-plasmon resonance. In addition, the mode will completely disappear when its dispersion relation will enter the particle-hole continuum of excitations of the heavy (slow) species. Beyond this point, the mode is severely damped and does not exist as a collective excitation anymore. The corresponding wave vector q^* can be determined by matching the energy of the acoustic plasmon $\omega = c_{ac}q$, taking into account a width of order $\tau^{-1}q$ with the edge of the particle-hole spectrum $q(q + 2k_{Fh})/2m_h$. An estimate of this wave vector is thus

$$q^* \simeq 2m_h[c_{ac} - V_{Fh} - \tau^{-1}]. \tag{16}$$

This condition is essentially similar to the one for k_c in Ref. 21 (where $V_{Fs}q$ and $2k_{Fs}$ were taken as energy and momentum units).

Correspondingly, q^* defines an energy and temperature scale,

$$T^* \sim c_{ac}q^*. \tag{17}$$

This temperature plays a role similar to the Debye temperature for acoustic phonons: there are no bosonic states to be occupied beyond. On the other hand, below this temperature, the physics of the system is affected by the existence of the extra collective mode—there are plasmon states whose occupation fluctuations can affect carrier mobilities. Based on the above, we see that we can potentially distinguish two very different temperature regimes:

(a) $T > T^*$. This is the high-temperature (HT) regime. In this regime, there is no collective mode and we can treat bismuth as a double Fermi liquid. We can thus deal with the electron-hole scattering in the usual way, for example, by solving the Boltzmann transport equation, or equivalent approximations. We will briefly discuss this rather conventional regime in Sec. II C.

(b) $T < T^*$. This is the low-temperature (LT) regime. In this regime, the presence of the acoustic plasmon plays a central role in the interactions among the particle. It will thus affect strongly the scattering between electrons and holes and lead to very different transport properties. The study of the consequences of such a mode is at the heart of the present paper and will be done for the resistivity in Sec. III, and in the subsequent sections for other transport coefficients.

C. High-temperature regime: Baber resistivity

Let us now examine the resistivity itself. As discussed above, we have to distinguish two different regimes of temperature. We examine in this section the high-temperature one, which shows relatively conventional transport properties, and will concentrate on the low-temperature regime in the next section.

At high temperature, no collective mode is present and thus we have two well-defined Fermi liquids. The resistivity is coming from the electron-hole interaction, since this is the only term that does not conserve the total current. Indeed, given the quadratic dispersion relation, the current is proportional to the momentum and thus the intraspecies interactions conserve the total current. The main source of resistivity in this regime is the Baber scattering,[11] which leads within a standard Boltzmann approximation to

$$\rho = \left(\frac{m_e m_h k_B}{3\pi e\hbar^3\sqrt{n}}\right)^2 W T^2 = AT^2, \tag{18}$$

where W is the electron-hole scattering rate, and n is the density of particles of a given species. This gives an approximation for the coefficient A of the T^2 term in the resistivity $\rho = AT^2$, which is usually the quantity extracted from experimental data. Thus, provided that one is able to compute W, we have a parameter-free fit for the experiment. The prefactor W was computed using a Thomas-Fermi approximation for the Coulomb interaction,[11] leading to

$$W = \frac{2\pi}{\hbar}\int_0^{2k_{Fs}} \frac{dq}{2k_{Fs}} V_{\mathrm{TF}}(q)^2[3(q/2k_{Fs})^2], \tag{19}$$

where k_{Fs} is the Fermi wave vector of the slower component. $V_{\mathrm{TF}}(q)$ is the Thomas-Fermi screened Coulomb interaction,

$$V_{\mathrm{eff}}(q) = \frac{4\pi e^2}{\epsilon_\infty q^2 + \kappa_{T-F}^{e2} + \kappa_{T-F}^{h2}}. \tag{20}$$

Reference[11] estimated the above terms using $\epsilon_\infty = 100$, $\kappa_{T-F}^i = 3(4m_i^2 k_{Fi}/\pi\hbar^2)$, where $m_e = 0.03, m_h = 0.15$, which were known from previous independent measurements. This led to $A = 8n\Omega$ cm K^{-2}, in good agreement with the experimental data of that time including $8n\Omega$ cm K^{-2} (reported in Ref. 27), $14.5n\Omega$ cm K^{-2} (in Ref. 8), and also the more recent ones[6,12] such as $12n\Omega$ cm K^{-2} for measurements along the binary axis. With the same formulas, an even better value of $A = 14n\Omega$ cm K^{-2} can be found if we use more recent values of parameters: $\epsilon_\infty = 88$, $m_e = 0.04$, and $m_h = 0.14$. The $Bi_{1-x}Sb_x$ compound, with $x = 0.037$ ($n_{x=0.037} \approx n_{x=0}/3$) was also measured,[7] and the experimental $A = 33n\Omega$ cm K^{-2} is in agreement with the expectations from (18), showing that the Baber scattering is indeed the good description of

the transport in this regime of parameters. However, low-temperature deviation from this simplistic picture was reported already in early works (see Ref. 9 for a detailed discussion).

Within the framework of the Baber scattering, one can go beyond the traditional Baber formula (18) in two ways. First, the large-temperature behavior can be computed as well.[28] At high enough temperature, the T^2 behavior of (18) crosses over, at a temperature of the order of $T_l \sim 0.2\sqrt{T_{Fe}T_{Fh}}$, to a linear temperature dependence. Experimental data in bismuth show that, indeed, above $T = 3$ K, there is a clear T^2 dependence, which becomes linear above $T = 25$ K. This is in reasonable agreement with the estimate given by the above formula, which for bismuth would be $T_1 \sim 35$ K. Second, one can refine the calculation of the coefficient A by taking into account the ellipsoidal character of the Fermi surface, rather than using the best fit for a spherical Fermi surface approximation ($m_e = 0.04$, $m_h = 0.14$). The procedure is given in Appendix B for the simplified case of two pockets only. The ratio of resistivities in different directions x and z is proportional to

$$\frac{\rho_x}{\rho_z} = \left[\frac{|m_{ex} - m_{hx}|/(m_{ex} + m_{hx})}{|m_{ez} - m_{hz}|/(m_{ez} + m_{hz})}\right]^2. \tag{21}$$

Given the masses of Table I, we expect that resistivity will be largest along the trigonal axis of the crystal. The asymmetry value of $\approx$1.4 that the above formula gives is slightly larger than the experimentally[8] found one of $\approx$1.15. However, one has to remember that due to highly anisotropic ellipsoids constituting the Fermi surface, the experiment requires a very precise monocrystal orientation.

However, the Baber scattering does not allow one to understand the low-temperature regime, which in bismuth corresponds to $T < 3$ K. For this regime, one has to invoke the existence of the acoustic plasmon. This is the regime that we consider now.

III. LOW-TEMPERATURE REGIME

As we mentioned in Sec. I, a previous attempt to describe the low-temperature regime invoked a coupling to a certain subspace of phonons.[13] To be precise, the authors took into account a cylindrical shape of Fermi (surface) pockets, and proposed a modified version of Bloch theory, where this strong anisotropy is taken into account while evaluating the momentum integrals. They were able to find a good fit of a resistivity in the range 0.4–1.5 K using reasonable values of three free parameters, although the necessary value of the electron-phonon interaction was two times bigger than now commonly approved in the literature.[29] There are, however, some other issues which give more substantial reason for doubts. First, phonons in this range have been proven to be ballistic by a thermal transport experiment.[6] Second, within the model, it is impossible to find a proper fit above 1.5 K, or more generally, to understand how low- and high-temperature regimes can be smoothly joined (as seen in all experiments).[8,9,12,27] Third, it is difficult to account for the anisotropy of resistivity.

We thus think that it is important to account for the low-temperature behavior of the resistivity to take into account the effects of interactions, and, in particular, the existence of the acoustic-plasmon mode discussed previously. This is what we examine now.

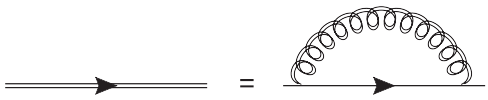

FIG. 3. The self-energy of a fermion (an electron or hole) experiencing a $V_{\rm eff}(q,\omega)$ interaction (a double coil, as in Fig. 2) during its propagation; as explained in the text, the effective interaction $V_{\rm eff}(q,\omega)$ is of the resonance form.

A. Effective Hamiltonian for lowest temperatures

As we determined in the previous section, at low enough temperature, an acoustic-plasmon mode exists. The very existence of this mode implies that for some values of the frequency and momenta, the effective interaction $V_{\rm eff}(q,\omega)$ between the carriers will have a pole. One can thus expect this pole to dominate the low-temperature transport.

In order to analyze the consequences of such a pole, we derive an effective low-energy Hamiltonian for which we consider this collective mode as a particle. This can be done by replacing the term corresponding to $V_{\rm eff}(q,\omega)$ (as shown in Fig. 3) by the propagator of a particle representing the bosonic fluctuations of the plasma, and ensuring that terms such as the self-energy terms, like the ones of Fig. 3, are correctly reproduced. Such a model is given by the coupling of electrons and holes to phononlike excitations,

$$H = H_0^h + H_0^e + \sum_q \omega_q b_q^\dagger b_q + \frac{1}{\sqrt{\Omega}} \sum_{\alpha=e,h} \sum_q M_q^\alpha [b_{-q}^\dagger + b_q] \rho_\alpha(q). \tag{22}$$

With such a Hamiltonian, the electron self-energy of Fig. 3 would be

$$\Sigma_e(q, i\nu_n) = -\frac{1}{\beta\Omega} \sum_{\omega_n, q} \left(M_q^e\right)^2 D(q, i\omega_n) \times \frac{1}{i\nu_n + i\omega_n - \xi_e(k+q)}, \tag{23}$$

where the ν_n and ω_n are the usual Matsubara frequencies, and $D(q,i\omega_n)$ is the phonon propagator:

$$D(q, i\omega_n) = -\frac{2\omega_q}{\omega_n^2 + \omega_q^2}. \tag{24}$$

The corresponding term for the original Hamiltonian is shown in Fig. 3 and is given by

$$\Sigma_e(q, i\nu_n) = -\frac{1}{\beta\Omega} \sum_{\omega_n, q} V_{\rm eff}(q, i\omega_n) \frac{1}{i\nu_n + i\omega_n - \xi_e(k+q)}. \tag{25}$$

One can show with this term, and the other diagrams, that the expansion is essentially identical, provided one identifies the proper "phonon" propagator and interaction vertex M_q. This can be done on the spectral function $A(q,\omega) = -\frac{1}{\pi}\mathrm{Im}D(q, i\omega_n \to \omega + i\delta)$. We only consider $\omega > 0$, since

$\omega < 0$ can be deduced from it. The "phonon" spectral function is

$$A_{ph}(q,\omega > 0) = \delta(\omega - \omega_q). \tag{26}$$

The effective potential $V_{\text{eff}}(q,\omega)$ of (9) is more difficult to evaluate fully. However, using the simple case of two types of particles (fast and slow) as discussed in Sec. II B, one has

$$V_{\text{eff}}(q,\omega) = \left(\frac{3\pi^2 m_r}{k_{Fr}^3}\right)\frac{1}{c_{ac}^2}1 - c_{ac}^2 q^2/\omega^2 + \imath\pi c_{ac}/2. \tag{27}$$

There is a finite lifetime due to the imaginary part (12), leading to a Lorentzian spectral function. If for the moment we ignore this finite width and assimilate the resonance to a δ-function peak, we have, for the spectral function,

$$A_{\text{plasmon}}(q,\omega > 0) = \left(\frac{3\pi^2 m_r}{k_{Fr}^3}\right)\frac{c_{ac}^3|q|}{2}\delta(\omega - c_{ac}|q|). \tag{28}$$

One can thus directly identify the two processes with

$$\omega_q = c_{ac}|q|, \quad M_q^{e0} = \left(\frac{3\pi^2 m_r c_{ac}^3}{2k_{Fr}^3}\right)^{1/2}|q|^{1/2}, \tag{29}$$

where M_q^{e0} is the zeroth-order approximation for the strength of electron-plasmon interaction [as introduced in Eq. (22)]. The above identification allows us to replace the problem of the screened Coulomb potential with a problem of electrons and holes interacting with a bosonic particle. This particle represents the quantization of the acoustic plasmon.

Let us make some comments on the validity of the identification (29). Obviously, the real calculation of the term $V_{\text{eff}}(q,\omega)$ or M_q^e, especially at finite temperature, would be more complex, and will certainly affect the quantitative aspects of the identification. However, we expect the *qualitative* features of the mode identification to be robust. In particular, the frequency of the acoustic plasmon will of course be linear in $u \sim q$ at small q, and in the same way, the matrix element describing the coupling to the particles will be $M_q^e \sim q^{1/2}$. Note that this specific dependence of the coupling constant is what makes the difference between the coupling to this acoustic-plasma mode and the coupling to normal acoustic phonons. This will have consequences for the temperature dependence of the resistivity that we will explore in the next section. The most drastic approximation that we made was to ignore the finite lifetime of the mode and to concentrate the full spectral weight in a δ-function peak. This approximation is not essential, and the finite lifetime can in principle be taken into account. It would simply correspond to a damping of the phonon mode. It simplifies, however, the subsequent calculations and allows one to extract the physics in a more transparent way, so we consistently use it in the remainder of this paper. On a quantitative level, both the broadening of the level $u''q$ and the average energy $u'q$ are proportional to q, as discussed in the previous section. For bismuth, a typical order of the ratio u''/u' is $u''/u' \approx 0.25$, so we expect such an approximation to be reasonably quantitative as well.

We can now use the standard diagrammatic analysis of electron-phonon interaction, keeping in mind the difference in the matrix elements, to obtain the various physical quantities when the acoustic plasmon is playing a major role. In particular, the self-energy (23) is simply given, after summation on the Matsubara frequencies, by

$$\Sigma_e(q,i\nu_n) = \frac{1}{\Omega}\sum_q \left(M_q^e\right)^2\left[\frac{b(\omega_q) + f(\xi(k+q))}{i\nu_n + \omega_q - \xi(k+q)} - \frac{b(-\omega_q) + f(\xi(k+q))}{i\nu_n - \omega_q - \xi(k+q)}\right]. \tag{30}$$

Since we are interested in the low-energy dissipation, we perform the analytical continuation $i\nu_n \to \nu + \imath\delta_+$, then the limit $\nu \to 0$, and finally extract the imaginary part of Σ_e. This last step leads to a δ function, which corresponds to a constraint, implemented to account for energy conservation [see, e.g., (40)]. This equation gives us a 2D surface Ω_0 of solutions q_0 for q. However, the above sum on q in (30) should be limited to the values for which the acoustic plasmon exists. We should thus only look at values of q lower than q^*, which was defined in (16). For small angles, only one of the masses dominates [see Eq. (B5)]. Combining this with (11) and the fact that we work in the $\omega \to 0$ limit, we deduce that in a limit of small angles (nearby direction of high symmetry), $c_{ac}(\theta) \sim \cos(\theta)$, which implies $q_0(\theta) = q^* \cos(\theta)$. Thus, one has always $q_0(\theta) \leqslant q^*$. Although potentially this criterion can depend on the direction of q, based on the above considerations, we can assume here that the directions of $\vec{q}$, where $q^*(\theta)$ drops to extraordinarily small values, are rare. In particular, this means that the surface Ω_0 is well defined. To obtain numerical responses, we will take an isotropic criterion for the upper cutoff.

B. New $\rho(T)$ dependence

In the low-temperature regime, the transport of the system, which is now dominated by the presence of the acoustic plasmon, can thus be described by the effective Hamiltonian (22). One has, to keep in mind that because of the unusual q dependence of the coupling to this bosonic degree of freedom (29), the temperature dependence of the resistivity is not necessarily the same as for the usual electron-phonon problem.

To compute the resistivity, we use the Kubo formula and express the resistivity as the current-current correlation function,

$$\text{Re}[\sigma_{xx}(\omega \to 0)] = \lim_{\omega\to 0}\frac{ne^2}{\omega}\text{Im}[\langle j_x(Q=0,\omega)j_x(-Q=0,0)\rangle]. \tag{31}$$

We are interested in the uniform response, so we set $Q = 0$; we will omit the x index in the following. The current is simply given by

$$J = \sum_{k,\alpha} e_\alpha \frac{k_x}{m_{x\alpha}} c_{k\alpha}^\dagger c_{k\alpha}, \tag{32}$$

where α is the particle species, and e_α and $m_{x\alpha}$ are the corresponding charge and mass in the direction of movement, respectively. The corresponding diagram is shown in Fig. 4(a), where the thick line and shaded triangle indicate that both propagator and interaction vertex are renormalized by $V_{\text{eff}}(q,\omega)$. The average in (31) will be computed with the effective Hamiltonian of the problem given by (22). It is important to

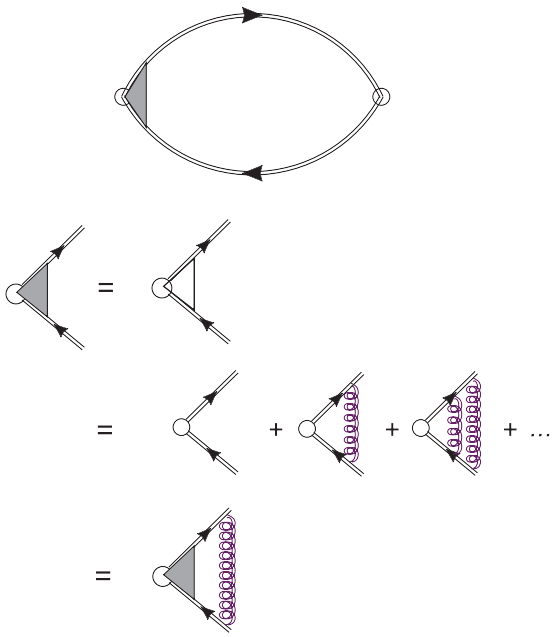

FIG. 4. (Color online) (top) The diagrammatic form of the current-current correlation function. The double line is the full Green's function for the electrons or holes, while the shaded box denotes the vertex correction that is shown in the bottom part. (bottom) The ladder series for vertex correction. The irreducible part consists of a single plasmon exchange (purple coil line) between the fermions (electrons or holes). For normal phonons, given the momentum dependence of the coupling constant M_q and propagator, it is crucial to include the vertex correction to get the proper temperature dependence.

note that given the topology of the diagrams entering the vertex corrections, there is indeed no double counting of diagrams if one replaces the thick coil of Fig. 4 by the bosonic excitation, as done in (22).

The procedure based on a development in power of the interaction in terms of diagrams is standard,[30] and follows closely the one for phonons. The vertex correction makes it cumbersome, so we give here a derivation based on the memory function that has the advantage of directly taking the vertex correction into account in a simpler way. The conductivity can be, in general, expressed as

$$\sigma(\omega) = \frac{i\chi_0}{\omega + M(\omega)}, \tag{33}$$

where χ_0 is the diamagnetic term, and $M(\omega)$ is defined as

$$M(\omega) = \frac{\langle F;F\rangle_\omega - \langle F;F\rangle_0}{-\chi(0)\omega}, \tag{34}$$

where the force F is $F = [j,H]$, and the $\langle F;F\rangle_\omega$ denotes the standard retarded correlation function at frequency ω. The averages are computed with the the part of the Hamiltonian that commutes with the current. Given that $M = 0$, if the current commutes with H, one recovers immediately in that case from (33) that the system is a perfect conductor. In particular, in the high-temperature regime, it shows immediately that the sole source of resistivity is the electron-hole interaction and the difference of masses between the two species.

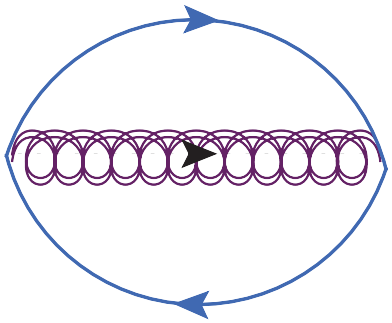

FIG. 5. (Color online) The force-force (F-F) correlation diagram. The solid blue line indicates the propagator of fermion (one, for example, slower component of the Fermi liquid), while the purple coil is the plasmon propagator.

On the contrary, the last term of Eq. (22) enters into the force F and thus leads to a finite resistivity. Evaluation of finite temperature averages (for independent fermions and bosons) will enable us to give the temperature dependence of this new resistivity component.

For low temperatures, in the case of the Hamiltonian (22) and using the definition of the current one (32), we obtain for F (for simplicity, we only kept two species, e and h),

$$F = \sum_{q,k,\alpha} e_\alpha M_{q\alpha} \frac{q_x}{m_\alpha} c^\dagger_{k+q,\alpha} c_{k,\alpha} [b^\dagger_{-q} + b_q]. \tag{35}$$

Each species gives thus a contribution to the force-force (F-F) correlation, which is shown in Fig. 5, and for Matsubara frequencies equal to

$$\langle F;F\rangle_{\omega_n} = \frac{1}{\beta^2\Omega^2} \sum_{\nu_1,\nu_2,k,q} \frac{M_q^2 q_x^2}{m^2} G(\nu_1,k) G(\nu_2,k+q) \times D(\omega_n + \nu_1 - \nu_2, q). \tag{36}$$

The frequency summation can be performed, which gives

$$\langle F;F\rangle_{\omega_n} = \frac{1}{\Omega^2} \sum_{k,q} \frac{M_q^2 q_x^2}{m^2} \times \frac{[f(\xi(k+q)) + b(-\omega_q)][f(\xi(k)) - f(\xi(k+q)+\omega_q)]}{i\omega_n + \xi(k) - \xi(k+q) - \omega_q} - (\omega_q \to -\omega_q). \tag{37}$$

After the analytic continuation, one gets, for the imaginary part of the function $M(\omega)$,

$$\mathrm{Im}M(\omega \to 0) = \frac{\pi}{\Omega^2} \sum_{k,q} \frac{M_q^2 q_x^2}{m^2} \frac{\partial f}{\partial \xi(k)} [f(\xi(k+q)) + b(-\omega_q)] \times \delta[\xi(k) - \xi(k+q) - \omega_q] - (\omega_q \to -\omega_q). \tag{38}$$

We are interested in the temperature dependence of the resistivity. We can thus, for simplicity, assume an averaged mass over the Fermi surface, which would affect the prefactor but not the temperature dependence. This allows one to replace

$q_x^2 \to q^2/3$. The term $\partial f/\partial\xi(k)$ constrains, at low temperature, to have k on the Fermi surface. One thus gets

$$\begin{aligned}\mathrm{Im}M(\omega\to 0) &= \frac{-k_F}{6\pi\Omega}\sum_q \frac{M_q^2 q^2}{m}[f(\xi(k_F+q)) + b(-\omega_q)] \\ &\quad\times \delta[\xi(k_F+q)+\omega_q] - (\omega_q \to -\omega_q) \\ &= \frac{k_F}{6\pi\Omega}\sum_q \frac{M_q^2 q^2}{m}[f(\omega_q)+b(\omega_q)] \\ &\quad\times \{\delta[\xi(k_F+q)+\omega_q]+\delta[\xi(k_F+q)-\omega_q]\}. \end{aligned} \tag{39}$$

If the temperature is small, the Fermi and Bose factors impose $qc_{ac} \sim T$, and thus the argument of the δ function simplifies to

$$\delta[\xi(k_F+q)+\omega_q] = \frac{k_F}{m}q\cos(\theta) \pm c_{ac}(\theta)q, \tag{40}$$

leading to

$$\mathrm{Im}M(\omega\to 0) = \frac{1}{6\pi}\int_{\Omega_0} dq \frac{M_q^2 q^3}{2\pi^2}[f(\omega_q)+b(\omega_q)], \tag{41}$$

where we applied the same reasoning as for the self-energy (30). The temperature can be rescaled out of the above integral, leading to

$$\mathrm{Im}M(\omega\to 0) = T^5\int_0^{\beta q^*} dq \frac{M_q^2 q^3}{12\pi^3}[\tilde{f}(\omega_q)+\tilde{b}(\omega_q)], \tag{42}$$

where the $\tilde{f}$ and $\tilde{b}$ are the Fermi and Bose factors, respectively, with $\beta = 1$, and we took the isotropic case. At low temperature, the integral tends to a constant, which can be evaluated in the isotropic case, so the resistivity has a temperature dependence given by

$$\rho(T) \propto T^5. \tag{43}$$

We thus see that the same electronic mechanism, which at higher temperature was giving the conventional Baber T^2 behavior, will smoothly lead to a T^5 behavior when acoustic plasmons begin to govern screening. The new T^5 behavior comes essentially from two approximations: the linear dispersion of bosons and $M_q \sim \sqrt{q}$. The upper limit of the integrals in (41) is the largest possible value of plasmon momentum. This critical wave vector q^*, at which Landau damping suppresses the plasmon as a well-defined particle, plays a role similar to the Brillouin zone boundary for acoustic phonons. As we discussed in Sec. I, one can also define a corresponding temperature T^* [see (17)], which is the analog of the Debye temperature and plays a similar role in the resistivity.

If we take a zeroth-order approximation for the interaction M_q^0 [see (29)] and $T^* \approx 1$ K, we can estimate the A coefficient in the Debye law [as defined in Eq. (1) of Ref. 12]. Along the trigonal axis, we get $A \approx 0.25\mu\Omega$ cm [in general, $A \in (0.25,0.6)\mu\Omega$ cm], which is not far from the experimental value $A \approx 0.15\mu\Omega$ cm. The zeroth-order approximation is overestimated because c_{ac}^0 (and also c_{ac}^{RPA}) is known to be overestimated, plus, as we explained, while evaluating the integral (41), the 2D surface of the solutions Ω_0 (for q) is not a full ellipsoid.

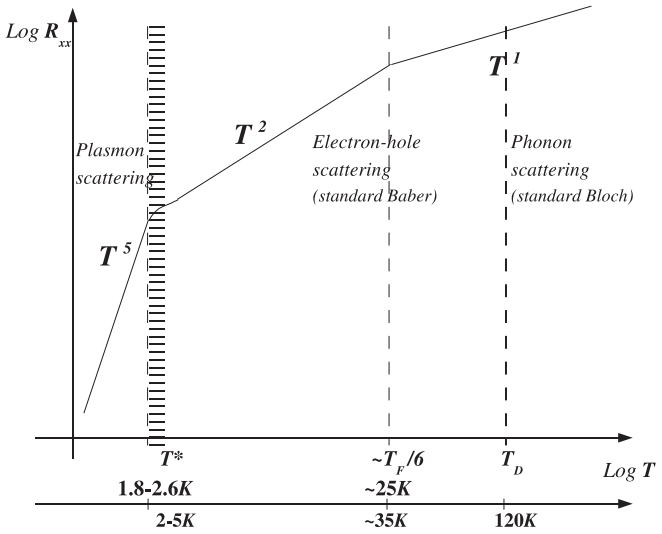

FIG. 6. The temperature dependence of resistivity in bismuth. Three power laws are distinguished: $\sim T^5$, $\sim T^2$, and $\sim T$. The lowest-temperature regime is due to the presence of the collective acoustic-plasmon mode. The two high-temperature power laws are either due to the conventional Baber scattering mechanism or (in the highest temperatures, above the Debye temperature T_D) due to scattering on phonons. On the additional temperature axis, the explicit values for bismuth are given. Both experimentally measured (upper) and theoretically evaluated (lower) values are indicated. The reason why the theoretical T^* is slightly overestimated is explained in the text.

A full temperature dependence of the resistivity is shown in Fig. 6. Note that the measured T^* will always be slightly smaller than the RPA value T_{RPA}^*, due to many plasmon processes (which are not accounted for in RPA) enhancing the Landau damping around T^*. In fact, one can expect that the RPA prediction T_{RPA}^* works better for polycrystal, where acoustic plasmons have more decay channels (for example, they can scatter on surface waves) as an alternative to Landau damping. This was indeed observed experimentally.[12]

Let us finally make a comment on the anisotropy of the resistivity to argue that the low-temperature conductivity is not strongly affected by a particular choice of $\vec{q}$ direction. In order to estimate the effect, we propose a zeroth-order approximation in which $\rho_{\vec{q}} \sim (M_q^0)_{\vec{q}}\langle b_{\vec{q}}^\dagger b_{\vec{q}}\rangle$, where an average is taken at a given low temperature. The direction dependence comes from the mass anisotropy and, in this respect, we know that two factors behave in different ways due to the following:

(i) From the reasoning given in Sec. III A, in particular (29),

$$\left(M_q^0\right)_{\vec{q}} \sim \left(c_{ac}^3\right)_{\vec{q}},$$

while at the lowest order, $c_{ac}^0 \sim V_{Fs} \sim (m_{s\vec{q}})^{-1/2}$, which implies

$$\left(M_q^0\right)_{\vec{q}} \sim (m_{s\vec{q}})^{-3/4}.$$

We expect this dependence to be stronger when we reach q^*.

(ii) The average density of plasmons $\langle b_{\vec{q}}^\dagger b_{\vec{q}}\rangle$ at the lowest temperatures will be determined by the Taylor expansion of the Bose-Einstein distribution $b[c_{ac}(\vec{q})q]$, which means $\langle b_{\vec{q}}^\dagger b_{\vec{q}}\rangle \sim m_{s\vec{q}}$, while at the higher temperatures (around $T \approx T^*$), the

density of available slow fermions (necessary to build up a collective excitation) sets the limit, which is also $\sim m_{s\vec{q}}$.

Both contributions to $\rho_{\vec{q}}$ scale in an opposite way with the mass, thus we expect the overall direction dependence to be rather weak (especially because a more refined approximation for $\rho_{\vec{q}}$ would need to contain some average over the whole Fermi surface).

We expect a stronger influence of anisotropy on q^* because this quantity depends only on the plasmon velocity $u = c_{ac} - \imath\tau^{-1}$. The problem is rather complex and we present a discussion of it in Appendix A. Considering the anisotropy of q^* brings us to an approximation we have made while deriving (42): we assumed that the plasmons propagate equally well in all directions. As shown in Appendix A, when more refined approximations for the polarizability $\Pi(k,\omega)$ are used, one gets more isotropic q^* values. Indeed, the measured anisotropy of T^* is quite weak.[12] This makes the derivation of (42) self-consistent.

C. Electron-plasmon coupling nonperturbative theory

As we saw in the previous sections, the presence of a collective mode has a drastic influence on transport properties. The mapping to the effective Hamiltonian (22) allows one to describe these effects. In the previous section, we looked at the consequences of such a coupling to the collective bosonic mode, in a lowest-order calculation in the self-energy.

However, it is well known for the case of electron-phonon coupling that the combination of the electrons and the phonon degrees of freedom can be carried out beyond this lowest order and leads to a new composite quasiparticle, the polaron. For the case of an acoustic plasmon, a similar phenomenon occurs.[31] In our case, the corresponding quasiparticle would be a plasmaron (electron accompanied by plasmons). The creation operator of a plasmaron can be written using a variant of the Lang-Firsov unitary transformation,

$$\tilde{c_k}^\dagger = c_k^\dagger \exp(-\hat{S}), \tag{44}$$

where

$$S = \sum_q \frac{\alpha_q}{e\hbar\omega_{q^*}} n_q (b_q^\dagger + b_{-q}), \tag{45}$$

in which $\alpha_q \sim M_q/E_F$ measures the strength of the boson-fermion coupling [in (45), we assumed it is real]. The shift of fermion energy ($\sim$Re$[\Sigma_{\text{boson}}]$) and mass ($\sim\partial_k$Re$[\Sigma_{\text{boson}}]$) are known as

$$|\Delta E| = (\alpha + 0.0123\alpha^2 + 0.00064\alpha^3 + \cdots)\omega_{q^*}, \tag{46}$$

$$\Delta m(\vec{q}) = (\alpha/6 + 0.024\alpha^2 + \cdots)m(\vec{q}), \tag{47}$$

where $m(\vec{q})$ indicates the mass in the $\vec{q}$ direction. The above formulas were obtained in the so-called large plasmaron picture. In the case of bismuth, the plasma is not rigid enough (contrary to the ionic lattice) to sustain self-localization, so a small plasmaron picture is unphysical.

Naturally, when $\alpha \to 0$, all the above effects disappear, but the question about the strength of the full M_q (not M_q^0) is open and quite difficult to access theoretically. We can only give an upper and lower limit for α. First, M_q must be smaller than the bare Coulomb interaction in order to make the plasmon a well-defined particle. The ratio of bare interaction to kinetic energy is given by r_s and, as discussed in detail in Sec. V A, $r_s \leqslant 1$, which implies $\alpha < 1$. The lower bound of α can be obtained experimentally: a recent optical spectroscopy measurement[4] showed the existence of an (optical) plasmaron in bismuth, which shows that the α coupling is sufficiently strong ($\alpha \sim 10^{-1}$) to give observable effects.

The notion of plasmaron allows for some developments of the theory beyond RPA. The numerical evaluation is left for future investigations. We will discuss some of these effects at the end of Sec. V A. However, a brief inspection of formulas (44)–(47) has several consequences:

(i) The dominance of the linear term in (46) and (47) confirms the accuracy of the first-order approximation for the electron-boson coupling, even for $\alpha \sim 1$, which validates our perturbative approach in M_q.

(ii) A plasmaron remains a well-defined fermionic particle, so the low-energy model (22) remains valid, but with renormalized parameters. We can thus expect the T^5 behavior of the resistivity to still be obeyed, even in an intermediate coupling regime.

(iii) From (47), we see that in the presence of a plasmon cloud, the mass of the heavier fermions further increases by Δm_s, which should give rise to a q^* increase. More importantly, the ratio of the geometric series that determines Δm_r is proportional to $\sqrt{m_r/m_r}$, which means that the effect is the strongest in the direction where q^* was smaller. Higher-order effects thus tend to stabilize the acoustic plasmon.

(iv) By definition (45), a fermion is mostly accompanied by plasmons propagating in the same direction ($\vec{q}_{\text{ferm}} \parallel \vec{q}_{\text{boson}}$); these plasmons are also mediating the effective interaction between electron and holes, and thus the part of interaction $\parallel \vec{q}_{\text{ferm}}$ is enhanced. This goes toward the unidirectional scenario advocated in Appendix A.

IV. OPTICAL SPECTROSCOPY: MAGNETOPLASMON

An obvious question is whether this new quasiparticle is responsible for the lowest-temperature resistivity data, and can be probed by other measurements.

Let us consider the consequences of the existence of the plasmon mode when there is a magnetic field acting on the system. We assume that the plasmon propagation direction is perpendicular to the external magnetic field, which is the geometry that is usually used in optical spectroscopy. We also assume that in this plane, electrons are heavier than holes (this can change depending upon the bismuth sample orientation). As we will see, the low-energy collective excitation can be probed by measuring the optical conductivity of the system.

A. Dispersion relation

The inconvenience of studying the acoustic plasmons with optical methods comes from the fact that in the limit $q \to 0$, which is the resonance condition with photons, by definition we have $\omega \to 0$. The way to overcome this difficulty is to introduce a magnetic field. In the case of a standard (optical) plasmon, the frequency of collective excitation (propagating perpendicular to the magnetic field) is increased by the magnetic field as $\omega = \sqrt{\omega_p^2 + \omega_c^2}$. This phenomenon can be explained intuitively: the movement of a charge under a

magnetic field requires an extra kinetic energy (to overcome the magnetic field vector potential). This result was found in several different ways: using RPA polarizability, the equation of motion technique, or from a simple hydrodynamic picture of fluctuations. The reason that such a remarkably simple relation holds comes from Kohn's theorem where, in a translationally invariant system for $q \to 0$, the magnetic field does not affect the interelectron interactions encoded in ω_p. Upon a detailed inspection of Kohn's derivation,[32] we see that in multicomponent plasmas, even embedded in a crystal lattice, the theorem holds approximately. In particular, in the case of bismuth, the deviations of cyclotron frequencies would be caused by electron-hole scattering with large momentum exchange. As we indicate in Sec. V A, due to the particular band structure of Bi, these contributions are suppressed and the theorem holds. It is thus still possible to provide a simple relation which links the (magneto)plasmon edge frequency with the plasma frequencies at zero field and the cyclotron frequencies (these last ones are known from the Kohn theorem).

Indeed, for the two-component plasma problem under a magnetic field, the following relation, valid for any value of the magnetic field in the $q \to 0$ limit, was found:[33]

$$\omega_{\pm}^2 = \tfrac{1}{2}\Big[\big(\omega_p^{e2} + \omega_p^{h2} + \omega_c^{e2} + \omega_c^{h2}\big) \pm \times \sqrt{\big(-\omega_p^{e2} + \omega_p^{h2} - \omega_c^{e2} + \omega_c^{h2}\big)^2 + 4\omega_p^{e2}\omega_p^{h2}}\Big]. \quad (48)$$

When $|\omega_c^e - \omega_c^h|$ is small, we find the intuitive relations $\omega_+^2 \approx \omega_p^{e2} + \omega_c^{e2} + \omega_p^{h2} + \omega_c^{h2}$ and $\omega_-^2 \approx |\omega_c^e \omega_c^h| + O(q)$, which allows for a clear identification of optical and acoustic plasmon when $B \to 0$. We see that the acoustic mode develops a gap, which should be observable in optics as a second, lower-frequency plasmon edge. In the limit when $|\omega_c^e - \omega_c^h| \gg |\omega_p^e|, |\omega_p^h|$, the $\omega_\pm$ modes in (48) become holelike and electronlike, respectively. It is relatively simple to reach this limit (when the second term under the square root is small) in bismuth. The reason is that we always have $m_r \ll m_s$, which implies that $|\omega_c^e - \omega_c^h| \sim |\omega_c^e|, |\omega_c^h|$. We thus expect ω_- to have an electronlike (in general, heavier particlelike) magnetic field dependence.

From (48), we can deduce how the frequency of the lower plasmon edge evolves with the magnetic field. The temperature dependence of $\omega_\pm$ is also frequently studied in optical experiments. The temperature dependence enters (48) via $\omega_p^{e,h} \sim n_{e,h}$. The density of carriers $n_{e,h}$ can change with temperature due to thermal excitation from the valence band. Because of the very small gap at the bottom of electron pockets, $\Delta \approx 13.7$ meV (see Fig. 1), this effect is particularly important for bismuth. Then a second type of holes as light as electrons will emerge, and due to the global compensation of electrons and holes, $n_e = n_h + n_{lh}$, the total number of carriers will increase. In the low-field limit, only the standard (high-energy) optical plasmon frequency $\omega_+(T)$ will be affected.

In the high-field limit, the ω_- will acquire a rather strong temperature dependence, since $\omega_-^2(T) \approx [\omega_p^e(T)]^2 + (\omega_c^e)^2$ (assuming that the electrons are heavier). From the charge neutrality condition, the approximate formula for $\omega_p^e(T)$ can be given[34] by

$$\big(\omega_p^e\big)^2 = \frac{4e^2}{\sqrt{2}\pi\hbar}\frac{\bar{m}_e^{3/2}}{m_x^e} Li_{1/2}\{\exp[\beta(-E_{Fe} - \mu)]\}(k_B T)^{3/2}, \quad (49)$$

where e is the electron charge, $\bar{m}_e$ is the geometrical average of electron masses, and m_x^e is a mass in a given direction (all masses in electron mass unit). $Li_{1/2}\{\exp[\beta(-E_{Fe} - \mu)]\}$ is the value of the incomplete polylogarithm function of the order $1/2$:

$$Li_{1/2}(a) = \int_0^\infty dx \frac{\sqrt{x}}{a\exp(x) + 1}. \quad (50)$$

This gives the temperature dependence of the ω_- for a very large magnetic field when this mode merges with the electron mode (in general, the heavier carrier mode).

B. Longitudinal *f*-sum rule

The third quantity accessible from optical measurements is the relative intensity of two-plasmon edges. This can be studied quantitatively using the longitudinal *f*-sum rule.

In a one-component plasma, it can be proven that the optical plasmon is the only collective excitation as $q \to 0$. It comes from an exact sum rule (see Ref. 30):

$$\int_0^\infty d\omega\omega \mathrm{Im}[\epsilon(q,\omega)^{-1}] = -\frac{\pi}{2}\omega_p^2. \quad (51)$$

An analog sum rule was derived for a multicomponent plasma (see, for example, Ref. 35). It was also shown[36] that in the presence of a nonlocal (q-dependent) potential, the right-hand side of (51) can change. This is particularly important for a two-component plasma when the nonlocal part might differentiate between intra- and intercomponent interactions [defined as $V_{\mathrm{eff}}^{\alpha\beta}(q)$ in (9)]. (Strictly speaking, in Bi, this is the case for $q \neq 0$, but arbitrarily small.) Then the sum rule is not completely exhausted by the ω_+ mode and there is some spectral weight left for the ω_- plasmon. [See also Ref. 26, where the acoustic-plasmon intensity increases for $d \neq 0$, a condition which in their case implies $V_{11}(q) \neq V_{12}(q)$.] These findings prove that the finite spectral weight of acoustic plasmon does not violate the longitudinal *f*-sum rule.

One can quantify this last statement by computing the strength of each plasmon, which in fact corresponds to $\mathrm{Im}[\Sigma_e(q)]$ evaluated in Sec. III A:

$$W_\pm(q) = \frac{\pi}{|\partial \mathrm{Re}[\epsilon(q,\omega)]/\partial\omega|_{\omega=\omega_\pm}}, \quad (52)$$

where $\epsilon(q,\omega)$ is a dielectric function defined as the denominator of Eq. (9), $\epsilon(q,\omega) = 1 - V_{\mathrm{Coul}}^{ee}(q)[\Pi_{hh}(q,\omega) + \Pi_{ee}(q,\omega)]$. By using the formulas given in Sec. II and the Lindhard approximation for polarizability, we find (in the $q \to 0$ limit)

$$\partial \mathrm{Re}[\epsilon(q \to 0,\omega)]/\partial\omega|_{\omega=\omega_-} \approx (r_v - R)\ln\left(\frac{\omega_- - V_{Fs}q}{\omega_- + V_{Fs}q}\right), \quad (53)$$

where r_v and R are characteristic, constant parameters of the two-component plasma (they are of the order of 1; for

precise definitions, see Appendix A). By taking into account $\lim_{B\to 0}\omega_- = c_{ac}q$ (neglecting Im[u]), we deduce that the numerator of the logarithm limits $W_-(q)$ as

$$\lim_{B\to 0} W_-(q) \sim \{(r_v - R)\ln[(c_{ac} - V_{Fs})q]\}^{-1}. \quad (54)$$

From (54), one recovers the Landau damping formula: when $c_{ac} \to V_{Fs}$, $W_- \to 0$. The larger c_{ac} is with respect to V_{Fs}, the larger spectral weight the acoustic plasmon will contain. From (54), we also see that when $c_{ac} \neq V_{Fs}$, the $W_-(q)$ is an increasing function of q; it is difficult to expand this formula in the $q \to 0$ limit, but using l'Hospital rules [for the derivative of $\ln(q)$], one can confirm our argument given in Sec.III A that $V_0^{ac} \sim q$.

The other implication of (52) is that inducing any gap in the $\omega_-(q=0)$ spectrum will increase $W_-(q=0)$. This is precisely what the magnetic field does, as shown in (48). In particular, in a strong magnetic field, $\omega_- \to \omega_c^e + \omega_p^e$, which means that the acoustic mode becomes a mode of heavier (electron in our example) plasma component. Then, there must be also a redistribution of the relative spectral weights of the two-plasmon edges $\omega_\pm$; the ω_- mode will be more and more pronounced. To be more precise in Eq. (52), to get the intensity of ω_- mode, we substitute $\epsilon(q,\omega)$ of the heavier component plasma. The $\mathrm{Re}\{\epsilon[q\to 0,\omega_-(q)]\} \to q^2$, so the denominator of (52) gradually approaches zero in the same way as $\mathrm{Re}\{\epsilon[q\to 0,\omega_+(q)]\}$. This resembles the fact that the spectral weight $W_-(q\to 0)$ must become as significant as $W_+(q\to 0)$. As the magnetic field increases, $W_-(q\to 0)$ gradually acquires all the density fluctuations of the heavier carriers.

C. Summary of the expected effects

The findings of two previous sections are summarized in Table II. In order to define the border between *low B* and *large B*, we define the ultraquantum (UQ) limit for which the magnetic field freezes the motion of carriers in a plane perpendicular to it. Then ω_c dominates over ω_p. Due to the particular band structure of bismuth and the field dependence of the chemical potential, electrons and holes enter the UQ regime at nearly the same field ($\approx 10T$). Thus the above-mentioned condition $|\omega_c^e - \omega_c^h| \ll \omega_p$ is valid up to quite high fields. The limit of validity of this condition is for smaller fields, but of the order of the ones of the UQ regime. The value will change depending upon whether one works with pure Bi or $Bi_{1-x}Sb_x$ ($x < 0.07$), where the UQ limit is reduced.

TABLE II. Summary of the expected field dependence of the two-plasmon edges. We present the magnetic and temperature dependencies of the lower-energy plasmon edge and the magnetic field dependence of its amplitude. The low- and high-field regimes are distinguished.

Property	Low B	Large B
$\omega_-(B)$	$\sim\sqrt{\lvert\omega_c^e\omega_c^h\rvert}$	$\sim\sqrt{(\omega_c^e)^2+(\omega_p^e)^2}$
$\omega_-(T)$	T independent	$\sim\omega_p^e(T)$
$W_-(B) = 1/\epsilon(\omega_-)$	$W_+ \gg W_- \sim B$	$W_- \to W_+$

There are effects not included in the above analysis. First, we observe that because of the charge neutrality requirement and the small value of the gap below the electron pocket, the chemical potential μ does depend on the magnetic field. Thus we expect

$$\mu(B) \Rightarrow n(B) \Rightarrow \Delta\omega_p^{e,h}(B), \quad (55)$$

but this extra dependence is significant only for fields above the UQ regime. In the same regime, one may also expect an anomalous Zeeman splitting and large magnetostriction, which in principle can change the band parameters (masses). A large spin-orbit coupling in bismuth is responsible for these effects. They are beyond the scope of this paper, which is dedicated rather to low-field effects, and we leave them for future investigations.

The other source of finite gap in the spectrum of acoustic plasmon at $q = 0$ is the finite tunneling probability $\Upsilon_\perp$ between two types of carriers (electrons and holes in our case). According to Ref. 26, the additional gap Δ_{SAS} (using the notations of this paper) will be proportional to the tunneling (or scattering) probability [see Eq. (26) in Ref. 26], $\Delta_{SAS} \sim \sqrt{V(q=0)\Upsilon_\perp}$.

Due to Bi band structure, the energy-momentum conservation strictly forbids such a scattering, thus $T = 0 \Rightarrow \Upsilon_\perp = 0 \Rightarrow \Delta_{SAS} = 0$. The situation could be slightly more complicated at finite temperature for which we can find a combination of energy-conserving states, but the conservation of $\vec{k}$ is still never fulfilled (electron and hole pockets are very far in momentum space). We conclude that these types of recombination processes, even in the higher-order scattering events, should not affect the zeroth-order prediction for $\omega_-(B\to 0, T) \to 0$ given before.

V. DISCUSSION

In this section, we want to discuss the limits of validity of our theory and the physics that can be expected when we reach those limits. The experimental relevance of these effects will be presented.

A. Validity of RPA

In order to assert the validity of analysis of the previous sections, which is mostly based on an the RPA of the interaction terms, it is important to estimate first the strength of these interactions in the case of bismuth. At ambient pressure, the ratio r_s of the potential energy to kinetic energy are, respectively, $r_s^e \approx 0.2$ and $r_s^h \approx 1.5$ for the electrons and the holes. These rather low values are due mostly due to very high dielectric constant of the background $\varepsilon_\infty = 88$. It is also important to note that a part of the Coulomb interaction, namely, the Hartree-Fock terms with exchange interaction $V_{\mathrm{Coul}}(q)/\epsilon_{TF}(q)$ with Thomas-Fermi screening, was already taken into account during self-consistent band-structure calculations, leading to renormalized dispersions $\varepsilon_{e,h}(k)$.[24]

Although this question is difficult to address quantitatively, it is useful to estimate if for the particular case of bismuth we could trust the RPA. Usually the following arguments are used to justify the RPA resummation shown in Fig. 3: (i) The small

number of carriers implies that the long-range character of interactions plays a major role [$V(q)$ large for $q \to 0$]. Then the diagrams with the largest divergence number (RPA series) are the most important. This is the case in bismuth despite the simultaneous validity of the "dense plasma" regime $r_s < 1$. (ii) We are primarily interested in the limit of long-wavelength excitations (below q^*), thus the influence of local-field effects is moderate.

In addition to these two arguments that support the RPA, the particular combination of band-structure parameters of bismuth contributes to a further suppression of the diagrams outside the RPA series. Indeed, in bismuth, the Fermi surface consists of distant pockets for electrons and for holes. A significant part of the exchange diagrams (the interpocket ones) requires quite large momentum exchange, so in the limit of small momenta as discussed above, [$V_{\text{eff}}(q \to \infty) \to 0$], their contribution must be very small. In addition, such processes are irrelevant in the Renormalization Group (RG) sense.[37] Another contributing factor comes from the fact that electrons along the trigonal axis can be considered as Dirac particles, while holes are very light in the perpendicular plane. If one takes a (one-component) gas of spinless fermions with linear dispersion, then the bubble approximation (each bubble with only two external interaction lines) works quite well. In particular, in one dimension, for such a Dirac (Tomonaga) spectrum, the RPA for interaction line would be exact. In particular, in one dimension, for such a Dirac spectrum, the RPA would be exact. In higher dimensions, one can thus expect that the amplitude of nonbubble diagrams should at least be reduced when $m \to 0$. Finally, both the large mass anisotropy (on the surface of each pocket) and the strong spin-orbit coupling [lowering the orbital momentum $\hat{j}_e$ quantum number ($\hat{j}_e = \hat{l}_e + \hat{s}_e$)] contribute to the weakening of the electron-electron exchange processes. Although none of these arguments are, of course, rigorous or final, they suggests that the RPA in bismuth is indeed a very good starting point to understand the properties of this material.

Improvement above the RPA is, of course, a very difficult proposal. Among the diagrams one would have to consider, are multiple acoustic-plasmon processes (optical plasmon has a high energy, so we can safely exclude it). Some of them are clearly suppressed. First, $M_q = 0$, which implies that tadpolelike diagrams mediated by acoustic plasmons give no contribution. Second, a multiplasmon scattering process has a natural cutoff q^*, above which they are strongly Landau damped. This mechanism of q^*_{eff} reduction was invoked in the context of Fig. 6. In fact, given the acoustic nature of plasmon excitation, one might be tempted to introduce a variant of the Migdal theorem in order to exclude processes with crossed plasmon lines. The Migdal theorem in our case has the following form: if we compare the available momentum phase space, we find that n-crossed multiplasmon lines will generate corrections proportional to $\lambda^n \omega_q / E_F$, where $\lambda \simeq M_q$. In order to estimate the value of the interaction, we note that the electron-plasmon coupling cannot be larger than the bare Coulomb interactions $\lambda < e^2 k_F \sim E_F$. Similarly, the energy transferred by the acoustic plasmons is of the order of $\omega_q \leqslant T^* < E_F$. Given the hierarchy of energies between T^* and E_F, we see that even without the large mass ratio that exists in the case of the electron-phonon coupling, here we have a justification of a Migdal-like theorem to drop the higher-order crossed plasmon diagrams.

Of course, even after excluding all of the above-mentioned processes, we are still left with many diagrams, which can be constructed around a dominating RPA series. The first class of multiplasmon diagrams which are left are the rainbow ones. Usually diagrams of this type are responsible for renormalization of particles' bare dispersion, which we have accounted for during the discussion of the plasmaron in Sec. III C. The second class of diagrams is the vertex corrections inside a single electronic bubble. The third class, which would make the problem highly nontrivial, corresponds to interactions between several electronic bubbles, which would lead to an interaction between the plasmon modes or interactions among several bubbles of the ladder series. The determination of how to take into account all of these terms is, of course, going well beyond the scope of the present study. Based on various arguments, one can expect, on a phenomenological level, a renormalization of the plasmon velocity. A phenomenological model that could account for those extra contributions would be to add an interaction term between the plasmons in our low-energy Hamiltonian (22) of the form

$$H_{pl-int} = \frac{1}{\Omega} \sum_{k_1,k_2,q} g(q) b^\dagger_{k_1+q} b^\dagger_{k_2-q} b_{k_1} b_{k_2}. \tag{56}$$

The interaction between plasmon term $g(q)$ can in principle be estimated from the above-mentioned diagrams, and this is left for a a future study. This phenomenological term could thus open the route to tackle the situation of $r_s > 1$.

B. Pressure-induced semimetal decay

One way to control the physics of the acoustic plasmon could be to consider the effect of pressure on these materials. Indeed, the tiny Fermi surface in bismuth is quite fragile versus Sb doping or pressure—the pockets empty and the material becomes a semiconductor. These dependencies are well established both on the theoretical (DFT pseudopotentials method in Ref. 38) and the experimental[39,40] side. Obviously, the collective excitations such as the plasmon will be affected by such a semimetal-semiconductor (SM-SC) transition.

At the first naive level, the change of carrier density affects only optical plasmon. The velocity c_{ac} (see Appendix A) depends on the ratio of masses and Fermi velocities of the two types of carriers. These crucial parameters, $m_{e,h}$ or $V_F^{e'h}$, seem to be constant up to very low carrier concentrations.[38] However, when $n \to 0$, the screening of the interaction is drastically affected and $r_s \to \infty$. The corrections beyond RPA, discussed in the previous section, start to be important. On the other hand, we know that at least for Sb doping, the gap (at L points) is being closed, thus ε_∞ increases, extending the validity of the "high-density plasma" regime. It means that it should still be possible to define plasmons as quasiparticles of the system, and the physics, which we described in the previous sections, should still be applicable.

Nontrivial effects may arise only near the critical doping δ_c or pressure p_c, for which $r_s \to \infty$. Two elements will play a role: (i) As described in the previous section (and at the end of Sec. III A), the most important effect emerging with an increasing r_s is the appearance of strong plasmon-plasmon

interactions. The interaction term (56) could potentially lead to an instability with a new minimum of the energy at a finite q. In that case, the corresponding energy gain would favor a semimetal (correlated liquid) versus a semiconductor. (ii) Contrary to $\omega_{ac}(q) = c_{ac}q$, the frequency of the optical plasmon $\omega_p \sim n$ is decreasing when $n \to 0$. At some point, the two collective excitations will merge. This should change both their dispersion as well as the physics of the system.

On the experimental side, the regime we are discussing above was recently studied by means of optical spectroscopy.[3] A transfer of the spectral weight to the plasmaron peak was observed. This implies that, as we expect, plasmons are able to survive (or can even be enhanced). In these experiments, a deviation from the Fermi liquid theory was found, with an abnormal rigidity of the metallic phase near p_c. What was observed can be interpreted as an abnormal increase of the collective-mode frequency (deviation from a single-mode RPA at the lowest temperatures). The extension of the theory proposed in the previous section, given by (56), can perhaps be used in such a regime to explain these effects.

C. Comparison with other multivalley semimetals

As already mentioned in Sec. I, a few other examples of the multivalley semimetals are known, with a band structure similar to bismuth. These other systems are thus potentially described by a similar theory to the one that we have introduced in this paper.

The most intensively studied material in this category is graphite. In this case, electrons and hole pockets are placed alongside, and are quite similar in shape, thus the carriers mass (and velocities) ratio is close to $\simeq 1$. In that case (see Appendix A), q^* shall be very small and the acoustic plasmons are always overdamped. The plasmonic regime predicted in this work does not apply in this case. We expect a standard Baber T^2 resistivity down to the lowest temperatures. This is indeed what is observed experimentally.[41]

The second material, which has been recently investigated, is 1T-$TiSe_2$. The band structure resembles strongly that of bismuth. It consists of three electrons and one hole pocket with large mass differences,[16] $m_h = 0.23$, $m_{ex} = 5.5$, $m_{ey} = 2.2$, and $\epsilon_\infty = 44$ (due to the large Se polarizability).[42] This suggests that we can have another family of materials where acoustic plasmons play a major role. The band structure gives a finite amount of acoustic plasmons in the system ($k^* \neq 0$), but also a quite large r_s, which resembles the situation described in Sec. V B more than the one of pure bismuth. This is most likely the reason why experimentally the low-energy physics of 1T-$TiSe_2$ is different than in Bi.

At T_{DW}, an electron liquid undergoes a density wave transition (accompanied by structural reconstruction). A superconducting transition subsequently takes place at T_{SC} if high pressure is applied or upon Cu intercalation. At the optimal pressure $p_c = 3$ GPa, $T_{SC} = 1.8$ K. The T_{DW} is quite susceptible to applied pressure, and drops from $T_{DW} = 200$ K (at $p = 0$) to $T_{DW} < 70$ K (at $p = p_c$). The density wave (DW) transition has a significant electron component, as revealed by angle-resolved photoemission spectroscopy (ARPES) measurements[16] (at $T = 63$ K), showing related reconstruction of the Fermi surface. Interestingly, the unusual increase of resistivity[43] which begins just above the T_{DW} seems to be similar to what was observed in Bi very close to the critical pressure p_c (both were attributed to an increase of the electron-hole scattering rate at the transition). The formation of an excitonic liquid was suggested to explain the transition at T_{DW}. Whether one can relate such an excitonic liquid description with the interacting plasmon theory that we described in the previous section is a challenging theoretical question that we leave for future studies.

VI. CONCLUSION

We have presented in this paper a theory of transport in semimetals, concentrating specifically on the case of bismuth. We have shown that the physical properties of these systems are dominated by the presence of an acoustic-plasmon mode at low temperatures. This mode that we derived in an RPA of the interactions leads to a drastic change of the transport properties, in particular their temperature dependence, compared to the standard Baber mechanism, which is normally invoked for such materials. We showed, in particular, that it would lead to a T^5 behavior of the resistivity below a certain energy scale T^*, dependent on the interactions that we computed. Above this energy scale, a normal T^2-like behavior is recovered for the resistivity. Our results are in agreement with the observed resistivity in bismuth. We examined several other consequences of the existence of such a mode and showed that it would lead to a double-plasma edge in optical magnetotransport experiments. Recent measurements of the optical conductivity agree well with our predictions.

The main contribution of our paper is thus to show the importance of such a plasmon mode in these systems. This opens the way to many lines of work centered around the existence and role of such collective modes. First it is important to explore the consequences of these collective modes for other transport properties. One of the most important is, of course, the Nernst effect, which in bismuth is one of the largest reported. Analysis on how the plasmon modes can modify the Nernst transport is a nontrivial question that we plan to analyze in detail. Another important direction is to go beyond the RPA analysis. This is necessary to investigate other semimetals such as Sn-doped bismuth or 1T-$TiSe_2$, or to take into account the effects of pressure on bismuth. In those cases, the interactions between the plasmons play a more important role. We have suggested a phenomenological model, which can potentially be used to tackle these effects. However, its analysis is highly nontrivial and this will provide certainly an exciting line of investigation for the future.

APPENDIX A: ACOUSTIC PLASMONS IN BISMUTH

We give here some arguments and energy scales for the acoustic plasmons in bismuth.

The existence of acoustic plasmons was initially investigated for bismuth[21] by means of a simple spherical Fermi surface model with $m_s = m_h = 0.14$ and $m_r = m_e = 0.047$. Based on this approximation, it was concluded that the acoustic plasmon was very weak ($k_c = 0.02 k_{Fs}$), although the authors also mentioned in their conclusion the issue of Fermi-surface elipticity.

Solving this issue, while taking into account the full elipticity, is a formidable, albeit necessary, task, as is obvious when looking at the parameters given in Table I. The dispersion relation of the collective mode is given by (9), in which the full masses should be inserted in the $\Pi(q,\omega)$ functions. Since the dispersion is quadratic, one can in principle rescale the integration over k in (7). One thus has

$$\Pi^0_{\alpha\alpha}(q,\omega) = (m_{\alpha 1}m_{\alpha 2}m_{\alpha 3})^{1/2}\tilde{\Pi}^0 \times (q_1/\sqrt{m_{\alpha 1}},q_2/\sqrt{m_{\alpha 1}},q_3/\sqrt{m_{\alpha 3}},\omega), \quad \text{(A1)}$$

where $\tilde{\Pi}^0$ is the normal Lindhard function with all the masses set to 1. For the case where $\omega/\tilde{q} = c$ constant and $\tilde{q} \to 0$, the Lindhard function becomes particularly simple:

$$\tilde{\Pi}^0(\tilde{q} \to 0,\omega = c\tilde{q}) = \frac{\tilde{k}_F}{\pi^2}\left[-1 + \frac{s}{2}\log\left|\frac{1+s}{1-s}\right|\right] - \iota\frac{\tilde{k}_F s}{2\pi}\theta(1-s), \quad \text{(A2)}$$

where $\tilde{k}_F^2/2 = E_F$, which is the Fermi energy of the corresponding species. Note that the two Fermi energies are not necessarily the same for the two species of particles and must be determined by the neutrality condition. When going to higher-order diagrams (vertex corrections), one realizes that not all scattering directions are equally probable. This means that the coefficient in front of $\tilde{\Pi}$ in Eq. (A1) will change because it depends on the anisotropic mass tensor. However, the form of the Lindhard function should not be affected by this procedure, thus the functional dependence of the plasmon dispersion relations should remain unchanged.

One can thus try to simplify such an equation. An extension of RPA (eRPA), taking into account the ellipsoidal shape,[44] gives the approximation to compute c_{ac} by averaging the faster component on a spherical Fermi surface, while retaining the ellipsoidal shape of the heavier (slower) component. If one follows this procedure, for example, on the trigonal axis, for which the electrons are faster than holes, then we need to substitute $m_s = m_{h3} = 0.63$, which is already significantly larger than $m_s = 0.14$. In the direction perpendicular to trigonal, the situation is even more complex. Holes are quite heavy along the trigonal axis direction, which gives large spherical mass and suggests that they are always the slower component. However, they are very light in the perpendicular direction (see Table I). It is then easy to forget that electrons, while extremely light along the trigonal axis, are (even in average) significantly heavier than holes in any perpendicular direction. Therefore, to be able to do the average, a spherical approximation (even the eRPA) would thus need to assume an opposite mass order than it is in reality. This suggests that a different approach is necessary.

A simple average over a spherical Fermi surface comes from the summation over $\vec{k}$ present in $\Pi^0_\nu(\vec{q},\omega)$ and the assumption that all scattering directions are equally probable. This is directly connected to neglecting interactions between electrons and holes within a bubble, and, in particular, the vertex correction within the bubble coming from the Coulomb interaction. Given the long-range nature of the interaction, it is natural to expect that such corrections would enhance the small q scattering. We can thus expect that the weighted mass that enters our expression for the dispersion relation is closer to the mass along the direction of q, rather than the mass averaged equally over all angles.

TABLE III. The parameters R and r_v (see text for definition) of acoustic plasmon along the trigonal axis in the limit $q \to 0$. eRPA is an average taking partially into account the ellipsoidal shape of the Fermi surface, while UD is a purely unidirectional approximation. The good agreement between these two extreme cases suggests that the corresponding results are probably representative of the experimental values in bismuth.

	R	r_v	c_{ac}	τ^{-1}	k^*
eRPA	11	0.2	1.8	0.4	0.25
UD	17	0.14	2.1	0.45	0.3

Although a full calculation is difficult and clearly beyond the scope of the present paper, we can have an idea of the importance of such effects by comparing to limiting situations, for the case of q along the trigonal axis. We take, on one hand, the averaging of the eRPA[44] and, on the other hand, the unidirectional (UD) approximation where we simply retain the mass along $\vec{q}$ while computing full polarizability. For an isotropic case, the expressions (9) considerably simplify and allow one to define two important parameters for the equation, namely, the relative weight between the two terms $R = (\kappa^s_{T-F}/\kappa^r_{T-F})^2 = (m_s k_{Fs})/(m_r k_{Fr})$ [where κ^i_{T-F} was defined in the context of Eq. (20)] and $r_v = V_{Fs}/V_{Fr}$, which is the ratio of the two velocities. The results are given in Table III.

We see that two extreme approximations give rather similar values. The correct values for bismuth should, therefore, be between these two extremes. This suggests that k^* is far from being negligible. Taking such values for k^* gives an energy of $T^* \approx 6$ K for the characteristic temperature below which the acoustic plasmon becomes strongly coherent.

In the perpendicular plane, the situation is significantly more complex. In fact, we have to work with a multiplasma problem given the three electron pockets so we can only give qualitative arguments. Let us stay within the UD approximation, remembering that it tends to slightly overestimate k^*. From Fig. 1, we immediately see that by changing the $\vec{q}$ direction, we are facing the following situation:

(i) There is one central hole pocket with an angle independent mass, $m_h^{1,2} = 0.067$.

(ii) The mass of each electron pocket can vary drastically, from very light ($m_e^2 = 0.0015$) up to the heaviest of all ($m_e^1 = 0.198$).

(iii) The electron pockets are situated with a relative orientation of $\pi/3$ and thus for every $\vec{q}$ direction, there are combinations with both very light and very heavy electrons present. This opens up the possibility for several plasmons to emerge, but most of them are strongly Landau damped. A rough estimation (for $\vec{q}$ not far from the bisectrix between two pockets) gives the following: for light hole-heavy electron, $R \approx 1.15 \Rightarrow k^* \approx 0.07$; for light electron-heavy hole, $R \approx 1.2 \Rightarrow k^* \approx 0.1$; and for light electron-heavy electron, $R \approx 13 \Rightarrow k^* \approx 0.22$. For another intermediate orientation ($\pi/6$ angle with the bisectrix), both electron masses will be smaller. A more precise evaluation of k^* would be quite difficult

and probably also susceptible to a significant error. Let us only emphasize that for the Fermi energies, $E_F^e \approx 2E_F^h$, thus a smaller value of k^* in the perpendicular plane does not immediately imply a smaller T^* in this plane.

Finally let us make two comments for plasmons far from the trigonal axis:

(1) If we had taken the eRPA approximation, we would have found rather low values of k^* along the bisectrix axis, which would imply a notable trigonal-bisectrix anisotropy of the observed T^*. This is not the case found experimentally.

(2) Due to the particular positioning of Fermi surface pockets, it is practically always possible to find carriers with rather different masses. Thus we expect that a drop of k^* for some directions is the exception rather than the rule. These rare cases should not affect significantly the $\vec{q}$ momentum integrals, such as the one in (41).

Note that in the above estimation of the T^* values, we have neglected local-field corrections. These always tend to reduce T^*.[45] To be precise, the larger k^*, the larger the influence of local-field corrections. This accounts for experimentally observed isotropy of T^* and explains why the "Debye" temperatures found by resistivity fits by Uher[12] are lower than the RPA expectations (a discrepancy that was already discussed in Sec. III B).

APPENDIX B: ANISOTROPY OF THE BABER RESISTIVITY

In order to compute the anisotropy of the resistivity due to the Baber scattering, we start from the formula obtained in Ref. 28 [Eq. (2.14) in that paper] and apply it to our problem with slow and rapid carriers:

$$\rho_x = \rho_0^x \beta \sum_{k,p,q} v_{pkq}^2 f(\xi_s(k))[1 - f(\xi_s(k) + \Delta_q)] f(\xi_r(p)) \times [1 - f(\xi_r(p) - \Delta_q)], \tag{B1}$$

where Δ_q is the energy exchanged in the scattering process (determined by the exchanged momenta q) and $\rho_0^x = \pi J^2/(\Omega D_x)$, with D_x being the density of carriers in a given direction and J being the strength of the carrier's interaction. In our model, instead of the J of Eq. (B1), included in ρ_0, the averaged scattering rate W must be substituted. Following the derivation of Ref. 28, we take the carriers velocity along the resistivity axis as the variational parameter $\Phi_{k^i} = V_x$. According to textbook procedure,[46] v_{pkq} is then equal to the total change of Φ_{k^i} during the scattering event, which in our case means $v_{pkq} = \Delta V_x$. When one derives the relation $\Delta V_x(q)$, one needs to take the masses along the x axis. The momentum along a given direction must be conserved, which implies that $|\Delta V_x(q)| \sim q_x |m_{ex}^{-1} - m_{hx}^{-1}|$, where q_x is the momentum exchanged along the resistivity axis.

The summation in (B1) is taken over vectors of incoming and outgoing carriers. The detailed, all-T treatment of (B1) would be quite complicated, but we are interested only in the lowest temperatures, where the energy exchanged during scattering goes to zero, $\Delta \to 0$ (we always stay on the Fermi surface), and the density of both electrons and holes is constant (the chemical potential in semimetal is rather stable). We also know from band structure that there is no nesting, $k_e \neq k_h$, and these Fermi wave vectors are also constant.

Note that the derivation in Ref. 28 was done for a two-dimensional system. Working in three dimensions requires one extra angle ϑ to complete the spherical coordinates. It is an angle between incoming momenta of light and heavy carriers between $\angle(\vec{k},\vec{p})$, which was obviously equal to zero for the 2D case. As long as we are interested in the resistivity along the high symmetry directions (which is the one usually measured) and in the limit of small Δ, we may assume that the functional relations $\Delta(\theta_{\vec{k}\vec{q}},\theta_{\vec{p}\vec{q}})$ and $|q|(\theta_{\vec{k}\vec{q}},\theta_{\vec{p}\vec{q}})$, originating from energy conservation, do not depend on the new angle ϑ. One integrates out this extra variable, but this does not change the low-energy T dependence (because the condition $\Delta \to 0$ allows one to give a unique relation between $\theta_{\vec{k}\vec{q}},\theta_{\vec{p}\vec{q}}$).

With the above remarks, we can evaluate the momentum sums, transposed into integral over the angles $\theta_{\vec{k}\vec{q}},\theta_{\vec{p}\vec{q}}$, ϑ. The masses $m_s(\theta_{\vec{k}\vec{q}})$ and $m_r(\theta_{\vec{p}\vec{q}})$, entering into the formulas accounting for energy conservation (during the scattering event), $\Delta(\theta_{\vec{k}\vec{q}},\theta_{\vec{p}\vec{q}})$ and $|q|(\theta_{\vec{k}\vec{q}},\theta_{\vec{p}\vec{q}})$, are averaged over all angles on the Fermi surface when integration over all possible orientations is taken. This brings us to an analog of Eq. (3.4) in Ref. 28 with the anisotropy factor extracted:

$$\rho_x = \frac{(\Delta V_x/q_x)^2}{D_x} \int d\theta_{\vec{k}\vec{q}} d\theta_{\vec{p}\vec{q}} d\vartheta q^2 \cos^2(\vartheta)[\cos(\theta_{\vec{k}\vec{q}}) - \cos(\theta_{\vec{p}\vec{q}})]^2 \frac{(\Delta_{\vec{q}}\beta)^2}{4\sinh^2(\Delta_{\vec{q}}\beta/2)}, \tag{B2}$$

where an integral is angle averaged, which also means averaged over all momenta on the Fermi surface. The integral is rather complicated in 3D. We can safely assume that the anisotropy of the resistivity is caused only by the two factors in front: a change of carriers velocity ΔV_x (along the resistivity direction) during the scattering event, which we already discussed above, and the denominator D_x. The denominator D_x is constant when $\mu(T) = cste$ and it introduces the probability of such a scattering event, which is proportional to the carrier density determined along the given direction by $D_x \sim (m_{ex}^{-1} + m_{hx}^{-1})^2$. The resistivity can be expressed as $\rho_x \sim |\Delta V_x|/D_x$. This implies that, in the low temperatures (when $\rho \sim T^2$), the main contribution to the anisotropy of resistivity is accounted for by the factor $|\Delta V_x|/D_x$, which after straightforward simplification gives

$$\rho_i(m_{ei},m_{hi}) = \left[\frac{|m_{ei} - m_{hi}|}{(m_{ei} + m_{hi})}\right]^2 I, \tag{B3}$$

where I is the angle-averaged integral. In the case of a two-pocket Fermi surface, this immediately leads to

$$\frac{\rho_x}{\rho_z} = \left[\frac{|m_{ex} - m_{hx}|/(m_{ex} + m_{hx})}{|m_{ez} - m_{hz}|/(m_{ez} + m_{hz})}\right]^2, \tag{B4}$$

where m_e and m_h are second-rank tensors with values (along the main axis) given in Table I. A reminder is necessary: the masses which are substituted into (21) are not the ones given in Table I. Indeed, the masses in (21) are the ones along the external directions, while Table I gives the ellipsoid

parameters. This point is particularly important for electrons along the trigonal axis: there is very small m_{3e}, but (due to out-of-bisectrix plane tilt ϑ of the electron ellipsoid) m_{ez} contains an admixture of relatively large m_{1e},

$$m_{ez}^{-1} = m_{3e}^{-1}\cos(\vartheta)^2 + m_{1e}^{-1}\sin(\vartheta)^2. \tag{B5}$$

There is one extra complication, which is present except when the selected direction is the trigonal one. It comes from the fact that in bismuth, we have more than two families of carriers. In the particular case of the bisectrix axis (along which resistivity is frequently measured), we have to deal with three different types of carriers (holes, light electrons, and heavy electrons) with certain probabilities for each type of scattering event. This leads to

$$\rho_x = \tfrac{3}{11}\rho_{1eh}(m_{e1},m_{h1}) + \tfrac{6}{11}\rho_{2eh}(m_{e2},m_{h1}) + \tfrac{2}{11}\rho_{ee}(m_{e1},m_{e2}), \tag{B6}$$

which one can compare with ρ_z measured along the trigonal axis; this is precisely what we did in Sec. II C.

[1] L. Schubnikov and W. J. de Haas, Nature (London) **126**, 500 (1930).
[2] W. J. de Haas and P. M. van Alphen, Proc. Netherlands Roy. Acad. Sci **33**, 1106 (1930).
[3] N. P. Armitage, Riccardo Tediosi, F. Lévy, E. Giannini, L. Forro, and D. van der Marel, Phys. Rev. Lett. **104**, 237401 (2010).
[4] Riccardo Tediosi, N. P. Armitage, E. Giannini, and D. van der Marel, Phys. Rev. Lett. **99**, 016406 (2007).
[5] C. Uher and W. P. Pratt Jr., J. Phys. F **8**, 1979 (1978).
[6] K. Behnia, M. A. Méasson, and Y. Kopelevich, Phys. Rev. Lett. **98**, 076603 (2007).
[7] A. Banerjee, B. Fauqué, K. Izawa, A. Miyake, I. Sheikin, J. Flouquet, B. Lenoir, and K. Behnia, Phys. Rev. B **78**, 161103 (2008).
[8] R. Hartman, Phys. Rev. **181**, 1070 (1969).
[9] C. A. Kukkonen and K. F. Sohn, J. Phys. F **7**, L193 (1977).
[10] W. Kraak, R. Herrmann, and H. Haupt, Phys. Status Solidi B **109**, 785 (1982).
[11] C. A. Kukkonen and P. F. Maldague, J. Phys. F **6**, L301 (1976).
[12] C. Uher and W. P. Pratt, Phys. Rev. Lett. **39**, 491 (1977).
[13] C. A. Kukkonen, Phys. Rev. B **18**, 1849 (1978).
[14] J. M. Schneider, M. Orlita, M. Potemski, and D. K. Maude, Phys. Rev. Lett. **102**, 166403 (2009).
[15] Z. Zhu, H. Yang, B. Fauque, Y. Kopelevich, and K. Behnia, Nature Phys. **6**, 26 (2009).
[16] H. Cercellier, C. Monney, F. Clerc, C. Battaglia, L. Despont, M. G. Garnier, H. Beck, P. Aebi, L. Patthey, H. Berger, and L. Forró, Phys. Rev. Lett. **99**, 146403 (2007).
[17] A. F. Kusmartseva, B. Sipos, H. Berger, L. Forró, and E. Tutiš, Phys. Rev. Lett. **103**, 236401 (2009).
[18] D. Pines and J. R. Schrieffer, Phys. Rev. **125**, 804 (1962).
[19] J. Ruvalds, Adv. Phys. **30**, 677 (1981).
[20] A. A. Cottey, J. Phys. F **15**, L203 (1985).
[21] B. Bennacer, A. A. Cottey, and J. Senkiw, J. Phys. Condens. Matter **1**, 8877 (1989).
[22] W. G. Baber, Proc. R. Soc. London A **158**, 383 (1937).
[23] R. Tediosi, Ph.D. thesis, Universite de Geneve, 2008.
[24] Yi Liu and R. E. Allen, Phys. Rev. B **52**, 1566 (1995).
[25] This is only an approximate separation because of the lack of inversion symmetry in this case. Experimentally it is usually found to be a good approximation in bismuth as long as there are no magnetic field or interface effects.
[26] S. DasSarma and E. H. Hwang, Phys. Rev. B **59**, 10730 (1999).
[27] E. W. Fenton, J. P. Jan, Å. Karlsson, and R. Singer, Phys. Rev. **184**, 663 (1969).
[28] T. Giamarchi and B. S. Shastry, Phys. Rev. B **46**, 5528 (1992).
[29] O. Hansen, I. Mikhail, M. Lavrenyuk, and N. Minina, J. Low Temp. Phys. **95**, 481 (1994).
[30] G. D. Mahan, *Many-Particle Physics*, *Physics of Solids and Liquids* (Kluwer/Plenum, New York, 2000), p. 358.
[31] G. Whitfield and P. M. Platzman, Phys. Rev. B **6**, 3987 (1972).
[32] W. Kohn, Phys. Rev. **123**, 1242 (1961).
[33] H. Noto, J. Phys. Soc. Jpn. **36**, 1137 (1974).
[34] D. van der Marel, R Tediosi, and F. Lévy (unpublished).
[35] H. Reinholz, R. Redmer, G. Röpke, and A. Wierling, Phys. Rev. E **62**, 5648 (2000).
[36] B. Adolph, V. I. Gavrilenko, K. Tenelsen, F. Bechstedt, and R. Del Sole, Phys. Rev. B **53**, 9797 (1996).
[37] A. A. Abrikosov, J. Low Temp. Phys. **10**, 1 (1973).
[38] B. Norin, Phys. Scr. **15**, 341 (1977).
[39] D. Balla and B. Brandt, Sov. Phys. JETP **20**, 1111 (1965).
[40] E. E. Mendez, A. Misu, and M. S. Dresselhaus, Phys. Rev. B **24**, 639 (1981).
[41] D. T. Morelli and C. Uher, Phys. Rev. B **30**, 1080 (1984).
[42] J. A. Wilson, A. S. Barker, F. J. Di Salvo, and J. A. Ditzenberger, Phys. Rev. B **18**, 2866 (1978).
[43] F. Levy, J. Phys. C **12**, 3725 (1979).
[44] B. Bennacer and A. A. Cottey, Semicond. Sci. Technol. **7**, 822 (1992).
[45] G. Vignale, Phys. Rev. B **38**, 811 (1988).
[46] J. M. Ziman, *Electrons and Phonons* (Clarendon, Oxford, (1962), p. 283.